

GA-A23130

CONF-990411--

ELECTRON CYCLOTRON CURRENT DRIVE IN DIII-D

by

T.C. LUCE, Y.R. LIN-LIU, R.W. HARVEY,
G. GIRUZZI, J.M. LOHR, C.C. PETTY,
P.A. POLITZER, R. PRATER, and B.W. RICE

DISTRIBUTION OF THIS DOCUMENT IS UNLIMITED

MASTER

RECEIVED

JUN 01 1999

OSTJ

MAY 1999

 **GENERAL ATOMICS**

DISCLAIMER

This report was prepared as an account of work sponsored by an agency of the United States Government. Neither the United States Government nor any agency thereof, nor any of their employees, make any warranty, express or implied, or assumes any legal liability or responsibility for the accuracy, completeness, or usefulness of any information, apparatus, product, or process disclosed, or represents that its use would not infringe privately owned rights. Reference herein to any specific commercial product, process, or service by trade name, trademark, manufacturer, or otherwise does not necessarily constitute or imply its endorsement, recommendation, or favoring by the United States Government or any agency thereof. The views and opinions of authors expressed herein do not necessarily state or reflect those of the United States Government or any agency thereof.

DISCLAIMER

Portions of this document may be illegible in electronic image products. Images are produced from the best available original document.

ELECTRON CYCLOTRON CURRENT DRIVE IN DIII-D

by

T.C. LUCE, Y.R. LIN-LIU, R.W. HARVEY,¹
G. GIRUZZI,² J.M. LOHR, C.C. PETTY,
P.A. POLITZER, R. PRATER, and B.W. RICE³

This is a preprint of an invited paper presented at the 13th
Topical Conference on Applications of Radio Frequency
Power to Plasmas, April 12-14, 1999, Annapolis, Maryland,
and to be printed in the *Proceedings*.

Work supported by
U.S. Department of Energy Contracts
DE-AC03-99ER54463 and W-7405-ENG-48

¹CompX

²CEA, Centre d'Études de Cadarache

³Lawrence Livermore National Laboratory

GENERAL ATOMICS PROJECT 30033
MAY 1999

Electron Cyclotron Current Drive in DIII-D

T.C. Luce, Y.R. Lin-Liu, R.W. Harvey,¹ G. Giruzzi,² J.M. Lohr,
C.C. Petty, P.A. Politzer, R. Prater, and B.W. Rice³

General Atomics, P.O. Box 85608, San Diego, California 92186-5698

¹*CompX, 12839 Via Grimaldi, Del Mar, California 92014*

²*CEA, Centre d'Études de Cadarache, F-13108 Saint Paul les Durance, France*

³*Lawrence Livermore National Laboratory, Livermore, California 94551-9900*

Abstract. Clear measurements of the localized current density driven by electron cyclotron waves have been made on the DIII-D tokamak. Direct evidence of the current drive is seen on the internal magnetic field measurements by motional Stark effect spectroscopy. Comparison with theoretical calculations in the collisionless limit shows the experimental current drive exceeds the predictions by a substantial amount for currents driven near the half radius. In all cases the experimental current density profile is broader than the predicted one.

INTRODUCTION

Extension of tokamak discharges to steady state is a major goal of the worldwide controlled fusion effort. For conventional tokamak discharges, an efficient source of non-inductive current is needed to reduce the recirculating power and thereby increase the net electrical output. For advanced tokamaks, the requirement is much more stringent, in that the appropriate current profile must be maintained to retain the enhanced stability and confinement. Current drive by electron cyclotron waves (ECCD) has the potential to fulfill these roles in future devices due to the high predicted efficiency for plasmas with the electron temperatures expected in fusion power plants and the controllable localized deposition set largely by optics and diffraction limits, which are small due to the short wavelength of electron cyclotron waves (2–3 mm). ECCD has the further technical advantages of high power density transmission systems (1 GW/m² achieved) and the possibility of launching waves using structures far from the plasma since the waves propagate in vacuum. The experiments reported here represent the first measurements of local non-inductive current profiles away from the magnetic axis in a hot plasma.

EXPERIMENTAL CONDITIONS

For the experiments reported here, two gyrotron oscillators operating at 110 GHz were employed. The range of power delivered to the plasma was 0.95–1.14 MW for generated powers of 1.23–1.43 MW, giving a typical transmission efficiency of 75%–80%. Most of the non-transmitted power is lost in the matching optics unit which converts the non-Gaussian output from the gyrotron to a Gaussian beam suitable for coupling to waveguide. The power is transmitted to the tokamak by evacuated corrugated waveguide designed for low loss. The transmission line contains a pair of grooved miter bends which can be oriented to polarize the beam to nearly any linear or elliptical

polarization. The beam is launched into the tokamak using a pair of turning mirrors. For these current drive experiments, the final mirror has a toroidal facet angle of 19° to direct the beam in the direction to enhance the existing current for the standard operation of DIII-D. The poloidal aiming of the beam can be changed between tokamak pulses. Further information on the DIII-D system can be found in Ref. 1.

The EC waves at 110 GHz are absorbed in DIII-D near the second harmonic of the electron cyclotron frequency. Of the two possible polarizations for electromagnetic waves in the plasma, only the polarization corresponding to X mode for $k_{\parallel} = 0$ ($\vec{k} \perp \vec{B} \perp \vec{E}$) is strongly absorbed for the DIII-D conditions. For the finite k_{\parallel} needed for current drive, this polarization is nearly circular. To maximize the current drive, the in-line polarizers must be set to generate this polarization. Experiments to verify proper operation of this system have been successfully carried out and are reported in Ref. 2.

Discharges without MHD instabilities are needed to successfully apply the current drive analysis technique described below. To avoid sawteeth, a neutral beam is injected into the plasma during the current ramp to raise the temperature in order to delay the resistive evolution, as shown in Fig. 1. The discharge is biased upward to increase the H-mode threshold power, since the grad-B drift is downward; therefore, the H mode was avoided and there are no ELMs. Periods of non-diffusive evolution of the poloidal flux are observed, and are correlated with bursts of low- n MHD at very low amplitude. These seem to be related to the minimum q reaching a low-order rational value. These modes rapidly disappear after the crossing through the rational surfaces. Because the resistive evolution is slowed by the NB heating, sufficient time is available between such events to analyze the current drive with good accuracy.

CURRENT DRIVE ANALYSIS

The non-inductive current density is inferred from time sequences of magnetic equilibrium reconstructions [3]. The interior magnetic fields are measured directly by motional Stark effect (MSE) spectroscopy of the deuterium atoms injected by the same neutral beam used to slow the resistive evolution [4]. The MSE data and the magnetics signals are used as constraints on solutions to the Grad-Shafranov equation. The result is a map of poloidal flux ψ as a function of space and time. Spatial derivatives of ψ give the current density parallel to the magnetic field (J_{\parallel}) as function of ρ , the square root of the toroidal flux normalized to its edge value. The time derivative of ψ at fixed ρ gives the electric field parallel to the magnetic field (E_{\parallel}). Assuming neoclassical conductivity (σ_{neo}) (validated in Ref. 3), the total non-inductive current density is given by $J_{\text{NI}} \equiv J_{\parallel} - \sigma_{\text{neo}} E_{\parallel}$. This includes bootstrap current, neutral beam current, and electron cyclotron current. To isolate the effect of ECCD, the results are compared to those from a discharge with only neutral beam and bootstrap current, and the difference in J_{NI} for these two cases is attributed to ECCD. The small differences in electron density (n), electron temperature (T_e), or impurity content (Z_{eff}) are taken into account by adjusting the J_{NI} in the fiducial discharge by the theoretical scaling. Note that the absolute value and distribution of theoretical non-inductive current is not used in the correction; only the ratio is applied. This correction is usually a small fraction of the J_{NI} for the fiducial.

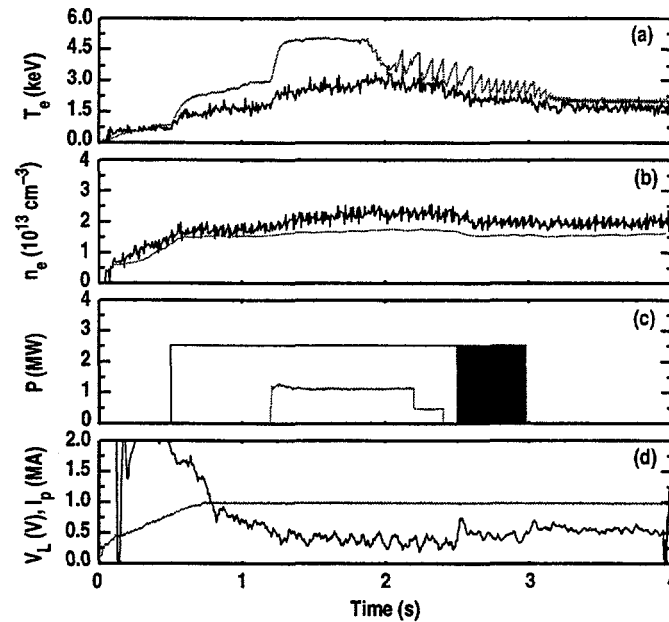


FIGURE 1. Time history of a typical ECCD discharge. (a) Electron temperature from central ECE (upper trace) and Thomson scattering near $\rho = 0.25$. (b) Electron density from Thomson scattering near $\rho = 0.25$ (upper trace) and line-averaged CO₂ laser interferometry. (c) Neutral beam power (upper trace) and EC power (arbitrary units). (d) Loop voltage and plasma current.

ECCD NEAR THE MAGNETIC AXIS

Application of the above technique to discharges with the intersection of the second harmonic resonance and the EC beam near $\rho = 0.2$ yields clear evidence of localized ECCD. The four steps of the analysis are shown in Fig. 2. The total J_{\parallel} is shown in Fig. 2(a) for both the ECCD and neutral beam only case. A clear modification of the current density is observed both at the predicted resonance location in ρ and interior to this. This modification is apparent even in the magnetic field pitch angles measured by MSE as shown in Fig. 3. The pitch angle is simply the angle whose tangent is the ratio of the poloidal to the toroidal field. In the absence of position and toroidal field changes, the time history of the pitch angle is proportional to the evolution of the enclosed current. In the ECCD case, it is clear qualitatively from the MSE pinch angles that the central current drops while the off-axis current density increases.

It may be somewhat surprising that the current density in the center can change so rapidly in a hot plasma. A resistive evolution simulation for a similar shot with resonance near the magnetic axis, shown in Fig. 4, indicates that a drop in the central current density and a rise at the resonance location are easily observed even at 100 ms into the EC pulse. The simulation uses a fixed geometry and kinetic profiles, and steps forward the neoclassical Ohm's law with the addition of a current source due to ECCD calculated from ray tracing and linear kinetic theory. The initial condition for the current density profile is taken to be the measurement at the time the EC power is turned on. The kinetic profiles are fixed to be those at the end of the ECCD analysis since this is the time of highest conductivity and therefore would impose an upper limit on the resistive evolution

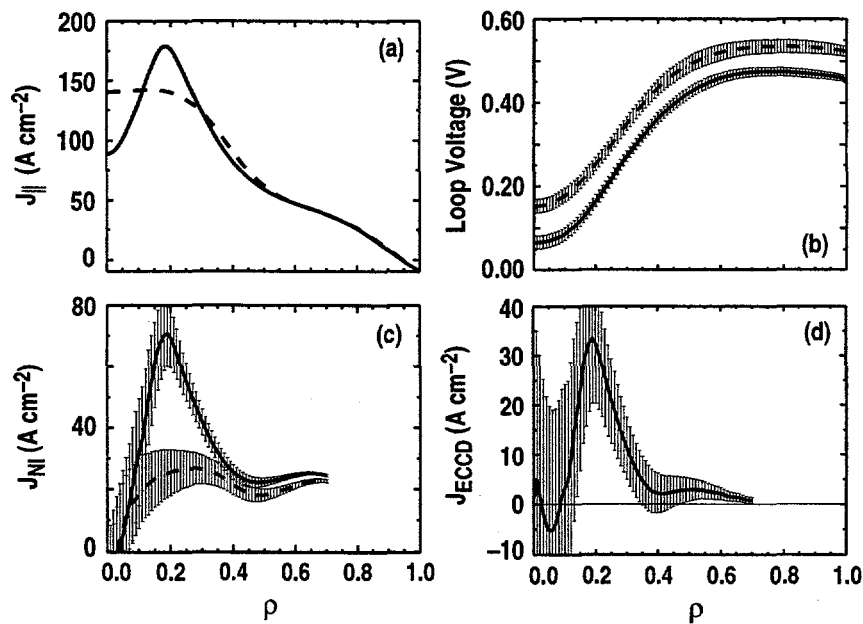


FIGURE 2. Analysis of the non-inductive current drive for the case near the magnetic axis. The plasma parameters are $B = 1.97$ T, $I = 0.98$ MA, $\bar{n} = 1.7 \times 10^{13}$ cm $^{-3}$, $P_{EC} = 1.03$ MW. (a) Total parallel current density, (b) loop voltage, (c) non-inductive current density, (d) electron cyclotron current density. In (a)–(c), the solid lines are the ECCD case and the dashed lines are the NB fiducial.

time scale. The simulation shows that the changes in J_{\parallel} seen in Fig. 2(a) are consistent with resistive evolution.

The change in the MSE pitch angles seen in Fig. 3 is, in principle, consistent with the generation of a radial electric field. However, the possibility that the EC waves generate a radial electric field rather than current drive can be ruled out. In addition to consistency with the neoclassical Ohm's law, it is possible to calculate the necessary change in toroidal rotation to change the MSE pitch angles by the observed amount. The observed change in the MSE pitch angles would require an order of magnitude increase in toroidal rotation while the measured toroidal rotation is unchanged or drops slightly. All of the direct measurements and consistency checks indicate the change in current density is due to ECCD.

The time behavior of ψ at fixed ρ gives the E_{\parallel} across the radius or equivalently the loop voltage ($V_L = 2\pi R E_{\parallel}$) shown in Fig. 2(b). The loop voltage is a true flux function. The error bars shown in Fig. 2(b) are the random errors in finding the slope of a straight line through the time sequence of equilibria at constant ρ to determine $\partial\psi/\partial t$. Typically, equilibria are generated at time slices 10 ms apart using 10 ms time averaging of the input data. The loop voltage is calculated every 10 ms using a fit over typically ± 100 ms around the time of interest. Shorter samples yield larger error bars, while longer samples can run into the problem that a straight line does not describe well the time history. The random error on the loop voltage is expected to dominate the random errors on J_{NI} , and the error bars in subsequent figures are the errors in the loop voltage propagated through the analysis. Note that in neither the ECCD nor the neutral beam case is the loop voltage close to equilibrium. This means that the standard loop voltage technique would fail to accurately determine the driven current in these cases.

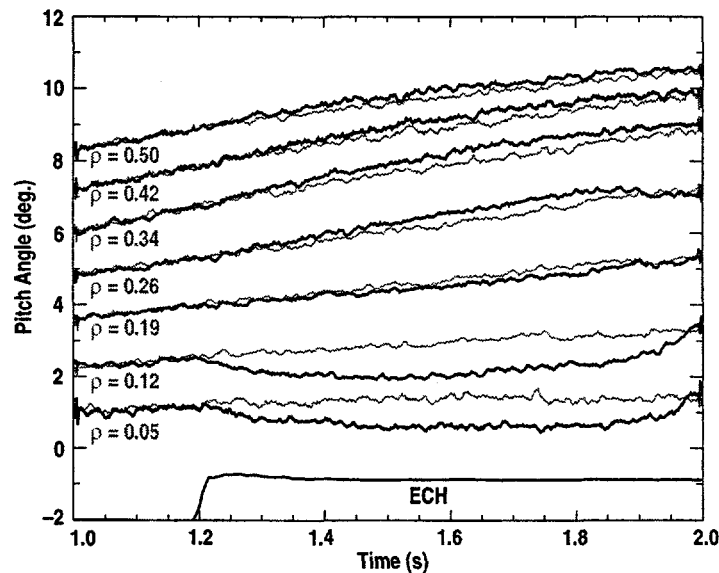


FIGURE 3. MSE pitch angle measurements versus time for the ECCD case (heavy line) shown in Fig. 2 and its NB fiducial (light line). Data are smoothed over 10 ms as used in the analysis.

The non-inductive current density clearly peaks, as shown in Fig. 2(c). Taking the difference with the neutral beam discharge shows a peaked ECCD profile at the resonance location [Fig. 2(d)]. The peak value is > 2 standard deviations (2σ) from zero, and there is more than 1σ from the peak to the half maximum. The total current is 48 ± 34 kA, where the error on the current is the integral of the area between the top of the error bars and the measured curve. This is a conservative estimate of the error.

The current (47 kA) predicted by a quasilinear Fokker-Planck calculation [5] using the measured kinetic parameters and the inferred E_{\parallel} is in excellent agreement with the measured value; however, the calculated profile is narrower than that measured in the experiment. At present, it is not possible to attribute the broadening in the measurement to the finite resolution of the analysis technique, broadening of the launched beam by some unknown effect, or transport of the fast electrons carrying the current. Efforts to assess the resolution of the analysis technique are underway.

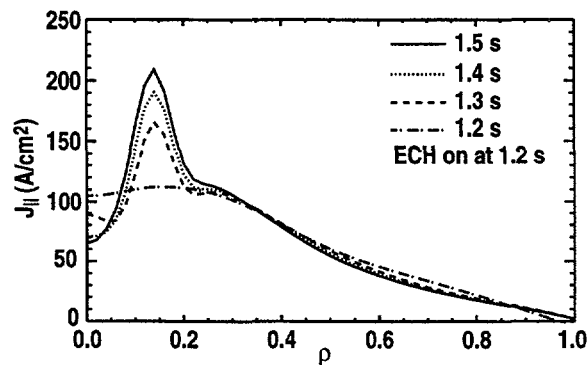


FIGURE 4. Results of a resistive diffusion simulation of the effects of ECCD near the magnetic axis. The j_{\parallel} at and interior to the resonance location change noticeably in the first 100 ms.

ECCD AT THE HALF RADIUS

Clear evidence of ECCD at the half radius is found using the same analysis technique applied above. Figure 5(a)–(d) shows the same for steps of the analysis described above. The modification of J_{\parallel} is much less because the local ECCD is less than the existing total J_{\parallel} , and any modification comes from the resistive diffusion. The main effect is that significantly less loop voltage is required to sustain the current profile [Fig. 5(b)].

The reduction in loop voltage can be seen directly in the MSE signals shown in Fig. 6. A rough estimate of E_{\parallel} is given by the toroidal component of Faraday's law:

$$E_{\phi} = \frac{1}{R} \int dR' R' \frac{\partial B_z}{\partial t}.$$

Assuming all of the change in the pitch angle is due to B_z , the reduction in the change in pitch angle indicates a smaller loop voltage on the ECCD case starting at $\rho \approx 0.25$. The calculation of J_{NI} [Fig. 5(c)] shows that this is due to a local addition of non-inductive current at exactly the location where ECCD is expected. This is clearly shown in Fig. 5(d) where the J_{EC} from the analysis is shown. Again, the error bars indicate a well-resolved peak in the measurement. As in the case with ECCD near the magnetic axis, the measured current profile is substantially broader than the predicted profile. However, in this case the total current is also substantially larger, 44 ± 19 kA versus 27 kA. The larger driven current in the analysis cannot be due to a finite resolution effect

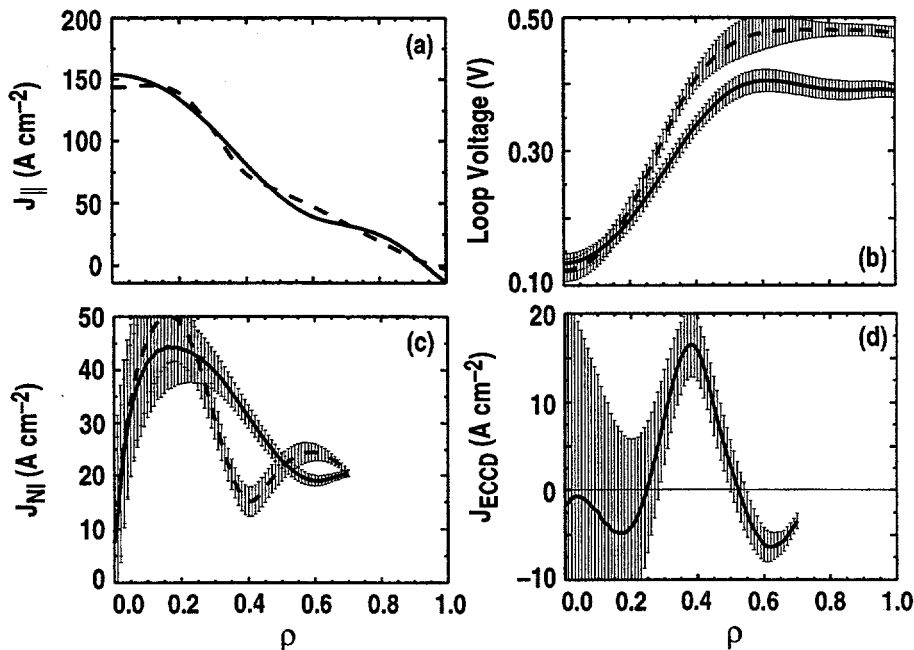


FIGURE 5. Analysis of the non-inductive current drive for the case near the half radius. The plasma parameters are $B = 1.76$ T, $I = 0.89$ MA, $\bar{n} = 1.8 \times 10^{13}$ cm^{-3} , $P_{\text{EC}} = 1.14$ MW. (a) Total parallel current density, (b) loop voltage, (c) non-inductive current density, (d) electron cyclotron current density. In (a)–(c), the solid lines are the ECCD case and the dashed lines are the NB fiducial.

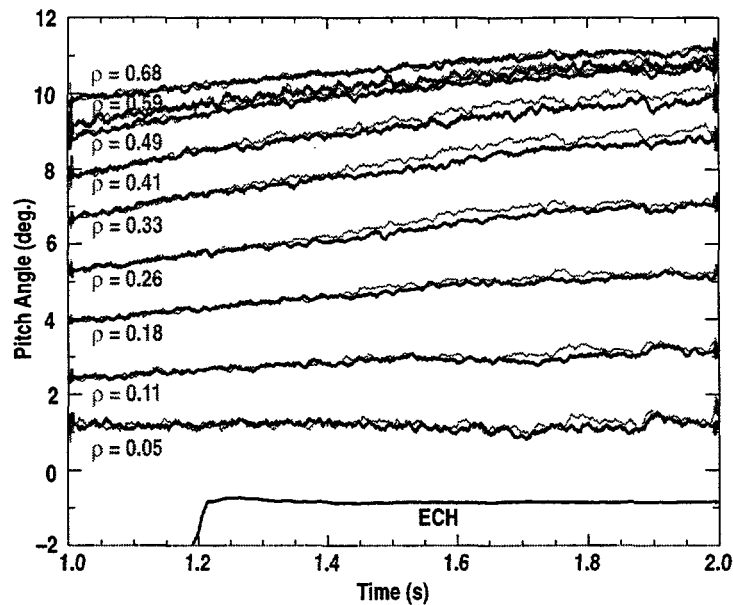


FIGURE 6. MSE pitch angle measurements versus time for the ECCD case shown in Fig. 5 (heavy line) and its NB fiducial (light line). Data are smoothed over 10 ms as used in the analysis.

since the analysis technique accounts for all of the applied poloidal flux by design. Any finite resolution effects can only redistribute current, not increase it.

COMPARISON TO THEORY

A detailed comparison to theory is presented in a separate publication [6] and only the results will be summarized here. The results presented in the previous two sections are typical of the entire ECCD experimental database. For cases with the resonance location at $\rho = 0.1$ – 0.3 , the measured current using the analysis technique described here and the predicted current using the quasilinear Fokker-Planck code are in very good agreement. For cases with $\rho = 0.3$ – 0.5 , the measured current is substantially higher than the prediction. In all cases, the measured profile is broader than the calculated profile. (The Fokker-Planck code employs a full ray-tracing calculation with multiple rays to model the refraction and finite-beam divergence effects.) Since the known temperature and density dependences are included in the calculation, it is postulated that the discrepancy is due to a simplified treatment of the trapped particle effects in the theoretical calculation. The effect of trapped particles is a subtractive effect (the “Ohkawa effect” [7]), so the impact of lessening the influence of trapped particles would be to add an offset to the theoretical predictions rather than a constant multiplier. Calculations to assess the current drive expected in the absence of trapped particles have been performed with the Fokker-Planck code by simply eliminating the magnetic well. The predicted current is in all cases much higher than the measured value, indicating that a reduction in the effective trapped electron fraction can explain the measurements. The leading candidate for a physical model is the inclusion of finite collisionality in the theoretical treatment. The standard Fokker-Planck treatment with a bounce-averaged collision operator does have a finite collision operator in all of velocity space, but imposes a strict boundary condition

between trapped and passing particles down to zero velocity. Clearly, this is not strictly true, and finite collisionality corrections could be significant since the first-order corrections are expected to scale with $\sqrt{v_*}$. The first analytic work in this area using an *ad hoc* connection formula to interpolate a linear adjoint response between the exactly tractable limits of collisionless and infinite connection length was reported at this meeting [8]. The enhancement of the predicted current drive efficiency is quite modest and is not enough to match the measurements. This linear adjoint approach does not include quasi-linear and E_{\parallel} effects. A full 3-D Fokker-Planck treatment with 2-D velocity space and 1-D along the magnetic field lines is in progress.

SUMMARY AND FUTURE PLANS

Localized ECCD out to the half radius has been clearly demonstrated in these proof-of-principle experiments. The effects indicated in the complete analysis can be directly observed in the MSE pitch angle measurements. The time scales for the observed current profile modifications are consistent with resistive evolution. The experiments indicate that the effect of trapped electrons is substantially less than that predicted by standard theory in the collisionless limit. Work is in progress to provide current drive predictions at arbitrary collisionality.

The near term plans are to begin experiments with an ELMing H-mode to test for possible mode conversion [9] or unexpected refractive effects. These experiments are a prelude to the first current profile control and tearing mode stabilization experiments.

ACKNOWLEDGMENT

This work was supported by the U.S. Department of Energy under Contracts DE-AC03-99ER54463 and W-7405-ENG-48.

REFERENCES

1. Callis, R.W., *et al.*, "The DIII-D 3 MW 110 GHz ECH System," this conference.
2. Petty, C.C., "Polarization, Propagation, and Deposition Measurements During ECCD Experiments on the DIII-D Tokamak," this conference.
3. Forest, C.B., *et al.*, Phys. Rev. Lett. **73**, 2244 (1994).
4. Rice, B.W., *et al.*, Phys Rev. Lett. **79**, 2394 (1997).
5. Harvey, R.W., McCoy, M.C., "The CQL3D Fokker-Planck Code," in *Advances in Simulation and Modeling of Thermonuclear Plasmas* (Proc. IAEA Technical Committee Meeting, Montreal, 1992), IAEA, Vienna (1993), p. 498.
6. Luce, T.C., *et al.*, "Generation of Localized Non-Inductive Current by Electron Cyclotron Waves on the DIII-D Tokamak," to be submitted to Physical Review Letters.
7. Ohkawa, T., "Steady-State Operation of Tokamaks by r-f Heating," General Atomics Report GA-A13847 (1976).
8. Lin-Liu, Y.R., *et al.*, "Modeling of Electron Cyclotron Current Drive Experiments on DIII-D," this conference.
9. Dumont, R., Giruzzi, G., Phys. Plasmas **6**, 660 (1999).